Article

GMars-T Enables Multimodal Subdiffraction Structural and Functional Fluorescence Imaging in Live Cells

Sheng Wang, Xuanze Chen, Lei Chang, Miao Ding, Ruiying Xue, Haifeng Duan, and Yujie Sun

Anal. Chem., **Just Accepted Manuscript** • DOI: 10.1021/acs.analchem.8b00418 • Publication Date (Web): 03 May 2018

GMars-T Enables Multimodal Subdiffraction Structural and Functional Fluorescence Imaging in Live Cells

Sheng Wang[a,1], Xuanze Chen[a,b,c,1], Lei Chang[a,1], Miao Ding[a], Ruiying Xue[a], Haifeng Duan[a] and Yujie Sun[a,*]

[a] *State Key Laboratory of Membrane Biology, Biodynamic Optical Imaging Center (BIOPIC),*

School of Life Sciences, Peking University, Beijing 100871, China

[b] *Department of Biomedical Engineering, College of Engineering, Peking University, Beijing 100871, China*

[c] *Cowin Venture Shanghai 200040, China*

[1] *Contributed equally to this work*

**Corresponding Author, sun_yujie@pku.edu.cn Phone number: 86-10-62744060*

ABSTRACT

Fluorescent probes with multimodal and multilevel imaging capabilities are highly valuable as imaging with such probes not only can obtain new layers of information but also enable cross-validation of results under different experimental conditions. In recent years, the development of genetically-encoded reversibly photoswitchable fluorescent proteins (RSFPs) has greatly promoted the application of various kinds of live-cell nanoscopy approaches, including reversible saturable optical fluorescence transitions (RESOLFT) and stochastic optical fluctuation imaging (SOFI). However, these two classes of live-cell nanoscopy approaches require different optical characteristics of specific RSFPs. In this work, we developed GMars-T, a monomeric bright green RSFP which can satisfy both RESOLFT and photochromic SOFI (pcSOFI) imaging in live cells. We further generated biosensor based on bimolecular fluorescence complementation (BiFC) of GMars-T which offers high specificity and sensitivity in detecting and visualizing various protein-protein interactions (PPIs) in different subcellular compartments under physiological conditions (*e.g.* 37℃) in live mammalian cells. Thus, the newly developed GMars-T can serve as both structural imaging probe with multimodal super-resolution imaging capability and functional imaging probe for reporting PPIs with high specificity and sensitivity based on its derived biosensor.

KEYWORDS: *GMars-T, RESOLFT, SOFI, BiFC, fluorescent protein, super-resolution fluorescence microscopy, reversible photoswitching*

INTRODUCTION

The engineering and applications of genetically-encoded fluorescent proteins and fluorescent protein-based (FP-based) biosensors have inspired the advancement of fluorescence bioimaging at two levels: (1) structure imaging which indicates the localizations and structure of FP-tagged biomolecules and (2) functional imaging which indicates spatial and temporal molecular dynamics and molecule interactions.[1] During last decade, the development of various photochromic fluorescent proteins including reversibly photoswitchable fluorescent proteins (RSFPs) has greatly promoted the applications of various super-resolution imaging techniques.[2-11] Adopting RSFPs as powerful imaging probes, two major approaches have been generally used for live-cell super-resolution imaging. One is based on reversible saturable optical fluorescence transitions (RESOLFT) concept, which operates with RSFPs requiring relatively low light intensity for saturation transition.[12] The other is based on photochromic stochastic optical fluctuation imaging (pcSOFI) concept, which operates with RSFPs displaying obvious temporal fluorescence fluctuations.[13] Although both approaches require that fluorescent probes such as RSFPs exhibit at least two different emission states (*e.g.* fluorescent and nonfluorescent states), the former relies on more controllable and target-coordinated photoswitching of fluorescent probes at ensemble level[14] while the latter relies on stochastic photoswitching of fluorescent probes at single pixel level.[15]

Although various RSFPs with special optical characteristics have been developed and optimized respectively for RESOLFT and pcSOFI imaging, there are still limited reports of a RSFP that can satisfy both nanoscopic imaging modes in live cells. In this work, we reported the development and characterization of GMars-T, a bright and monomeric green RSFP which can satisfy both RESOLFT and pcSOFI imaging in live cells. We further demonstrated high specificity and sensitivity bimolecular fluorescence complementation sensor based on GMars-T for detecting and visualizing PPIs under physiological conditions (*e.g.* 37℃) in live mammalian cells. These special features of GMars-T not only enable multimodal super-resolution

structural imaging but also high specificity functional imaging for reliably reporting PPIs in live cells. Thus the generation of GMars-T could expand the extremely valuable but limited RSFP toolbox specifically with both multimodal and multilevel imaging capabilities.[9]

EXPERIMENTAL SECTION

Generation of GMars-T based on mMaple3.

We generated green reversibly photoswitchable fluorescent protein GMars-T based on photoconvertible fluorescent protein mMaple3.[3] We first made M168A mutation to mMaple3 as conducted comparable M159A mutation in previous mEosFP,[16] and found that the resulting variant mMaple3(M168A) gain a new characteristic that is reversibly photoswitchable in its green and red form similar as previously reported IrisFP,[17] NijiFP[16] or pcDronpa.[9] we named this new variant as Mars for mMaple3 with reversibly switchable characteristics. We then made saturation mutations to the to the first amino acid of its chromophore tripeptide HYG as conducted in previous mGeos work[18] and produced a series of green reversibly photoswitchable fluorescent proteins, GMars (green form Mars). We selected a bright efficient photoswitching GMars variant named GMars-T (mMaple3 [H71T, M168A]) for detailed analysis in this work.

Plasmid Design and Construction.

We generated pGMars-T-N1and pGMars-T-C1 vectors by inserting GMars-T cDNA sequences into pEGFP-N1 (Clontech) and pEGFP-C1 (Clontech) vectors using BamHI/NotI and NheI/HindIII sites respectively to replace EGFP gene sequences. H2B cDNA sequences (*Homo sapines*) were inserted into pGMars-T-N1 vector. Lifeact sequences were PCR-amplified and tagged to the N-terminal cDNA sequences of GMars-T and then subcloned into pcDNA3.1 (+) vector with BamHI /EcoRI sites. ER targeting sequence KDEL or mitochondria targeting sequence was tagged to the C-terminal or N-terminal of GMars-T and subcloned into pcDNA3.1 (+)

vector with the same BamHI/EcoRI sites respectively. To construct EB3-GMars-T or LAMP1-GMars-T, the cDNA sequences of EB3 or LAMP1 were amplified and inserted into pGMars-T-N1 vector using NheI/HindIII sites. To construct GMars-T-N-β-Jun and β-Fos-GMars-T-C, the cDNA sequences were inserted into pcDNA3.1(+) vector using NheI/BamHI sites, the linker sequences were selected as 2×GGGGS and 4×GGGGS respectively. To construct GMars-T-N-FKBP and FRB-GMars-T-C, the cDNA sequences were inserted into pcDNA3.1 (+) vector using NheI/BamHI sites. The linker sequences were selected as 2×GGGGS and 4×GGGGS respectively. To construct GMars-T-N-Bak and Bcl-X_L-GMars-T-C, the cDNA sequence of GMars-T-N-Bak or Bcl-X_L-GMars-T-C was inserted into pcDNA3.1 (+) vector using NheI/BamHI sites with linker sequences as 2×GGGGS or 4×GGGGS respectively. The expression constructs for Lifeact-GMars-T-N, Lifeact-GMars-T-C, GMars-T-N-cofilin and actin-GMars-T-C were all established similarly.

Protein Expression and Purification.

GMars-T cDNA sequences were subcloned into pET15b (Novagen, Madison, WI) expression vector. Protein expression was conducted in E. *coli* strain BL21 (DE3) after induction with 0.4 mM isopropyl β-d-thiogalactoside (IPTG). Protein purification was performed using Ni^{2+}-nitrilotriacetate affinity resin (Ni-NTA; Qiagen, Hilden, Germany). The proteins were concentrated to about 10 mg/ml before further purification by size-exclusion chromatography using Superdex-200 column and Akta purifier system (GE Healthcare, Freiburg, Germany).

Measurements of Spectral Properties and p*K*a.

GMars-T spectral properties including absorption, excitation and emission were measured using a SpectraMax M5 (Molecular device, USA) Instrument. The fluorescence quantum yield (Φ_{Fl}) was determined relative to the reported value of fluorescein (quantum yield = 0.95 and molar extinction coefficient = 70,000 M^{-1} cm^{-1} at 491 nm). The extinction coefficient (ε) was determined using alkali-denatured method described previously.[19] For p*K*a measurements, protein solution were added

into glycine-hydrochloric acid buffer (for pH $\leqslant$ 5) or sodium phosphate buffer (for pH $\geqslant$ 6) with different pH values (2~11). The p*K*a value was taken as the pH value where the fluorescence emission reached 50% of the maximum.[2] The pH-dependent absorption was also measured as the method described above with buffers pH ranging from 3 to 11.

Cell Culture and Transfection.

U2OS and HeLa cells were cultured in DMEM complete medium (Gibco, Eggenstein, Germany) supplemented with 10% fetal bovine serum and maintained at 37°C and 5% CO_2 in a humidified incubator. Cells transient transfection was performed using Lipofectamine™ 2000 (Invitrogen Carlsbad, CA). For pcSOFI or RESOLFT imaging, cells were grown in IMEM (Gibco, Eggenstein, Germany) or DMEM complete medium without phenol red.

Measuring the photoswitching properties of RSFPs

An inverted fluorescent microscope (Olympus, IX81) was used to acquire images for photoswitching kinetics analysis. To activate and off-switch RSFPs, we used 405 nm light (25 W/cm^2) and 488 nm light (50 W/cm^2) alternatively. The off-switching time constant (τ) was determined by fitting the curve. Similarly, the off-switching halftimes under high illumination power were determined as a function of the off-switching light intensity using a Leica SP8 microscope equipped with a 100× NA 1.4 oil objective with a constant on-switching 405 nm light (25 kW/cm^2). The pixel dwell time for 405 nm light activation was 10 μs and off-switching 488 nm light was 1.2 μs. The activation time and off-switching light intensities were chosen to fully activate and switch off fluorescent proteins during each switching cycle. The residue fluorescence during each switching cycle was calculated and presented as a percentage value of remaining fluorescence intensity of on-state.

Dimerization Tendency Assay.

The oligomeric states of GMars-T were analyzed using Superdex 200 column and

Akta purifier system (GE Healthcare, Freiburg, Germany). The purified fluorescent proteins were diluted to 3-4 mg/ml. The UV absorption of proteins was recorded at 280 nm.

RESOLFT Nanoscopic Imaging.

RESOLFT experiments were carried out on a commercial parallelized RESOLFT microscope (2-color RESOLFT Parallel, Abberior Instruments, Germany). A 405 nm continuous wave diode laser was used for on-switching; 488 nm and 592nm continuous wave lasers were used for off-switching and fluorescence readout. A 100×, NA 1.45 oil-immersion objective lens (IX83, Olympus) was equipped for imaging. Two independent sCMOS cameras (Hamamatsu, Flash 4.0) were equipped for two-color RESOLFT microscope. Unless specified, RESOLFT images were always taken using 36 nm scanning step (pixel) size and $(360/36)^2$ steps are required for each frame. For GMars-T imaging, a 405 nm continuous wave diode laser was used for on-switching (2 ms); a 488 nm continuous wave laser was used for off-switching (15 ms); and fluorescence readout (4 ms). For rsCherryRev1.4[20] imaging, a 405 nm continuous wave diode laser was used for on-switching (2 ms); a 592 nm continuous wave laser was used for off-switching (80 ms) and fluorescence readout (10 ms).

Optical Setup and Data Processing for pcSOFI.

Fluorescence imaging was carried out on an inverted Nikon Eclipse Ti microscope (Nikon Instruments) with a TIRF objective (60×, 1.49 NA, Nikon) and additional 1.5× magnification, corresponding to a pixel size of 72 nm. Perfect Focus System (PFS) was used for reducing axial drift. Two lasers were used for excitation: 405 nm (200 mW nominal, Coherent Sapphire); 488 nm (200 mW nominal, MPB). The laser beam was coupled into the microscope objective using a multiband beam splitter (TRF89901-EM, 405, 488, 561, and 640 nm Laser Quad Band Set, Chroma Technology). The images were recorded using a sCMOS camera (sCMOS, Flash 4.0, Hamamatsu). For SOFI images, the raw data was first drift corrected[21] and then

second-order crosscumulant SOFI analysis with shortest lag time and Richardson–Lucy algorithm (3 iterations) was implemented using Localizer software package in Igor Pro (WaveMetrics).[22]

RESULTS AND DISCUSSION

We previously reported GMars-Q (mMaple3 [H71Q, M168A]), a monomeric green RSFP selected from the collection of GMars variants for long-term live-cell parallelized RESOLFT imaging.[5] Further screening of the GMars variants identified an even brighter and efficient photoswitching green RSFP termed GMars-T (mMaple3 [H71T, M168A]) with only one amino acid difference from GMars-Q. GMars-T has similar spectral characteristics (Figure 1a) as its predecessor mMaple3.[3] Interestingly, GMars-T showed markedly different pH-dependent absorption from GMars-Q (Figure 1b). While the p*K*a value of GMars-Q is 6.1, p*K*a value of GMars-T is 4.7 (Figure S1), making it especially useful for imaging acidic organelles in live cells. We next characterized the brightness of GMars-T. The ensemble measurement of purified proteins exhibited an extinction coefficient of $\varepsilon \approx 55{,}000\ M^{-1}cm^{-1}$ and a fluorescence quantum yield of $\Phi_{Fl} = 0.53$, indicating improved ensemble brightness ($\varepsilon \times \Phi_{Fl}$) of GMars-T compared with GMars-Q.[5]

Besides the ensemble brightness, the photoswitching characteristics at the ensemble level are also crucial for live-cell super-resolution imaging, especially for RESOLFT microscopy [4,23]. We next quantify these properties of GMars-T. As shown in Figure 1c, multiple photoswitching cycles were generated by alternating irradiation with 488 nm and 405 nm light and recorded in living cells expressing GMars-T, rsEGFP2 and rsEGFP(N205S), respectively (Figure 1d). The residual fluorescence was ~1% (n=10) for GMars-T similar as GMars-Q, which is 7~8 folds lower than that of rsEGFP2 or rsEGFP(N205S) in live cells. The off-switching halftimes of GMars-T measured under both low intensity light ($50 W/cm^2$, typically used for conventional wide-field fluorescence microscopy) and high intensity light (1-100 kW/cm^2, typically used for RESOLFT, PALM and Confocal microscopy) were slightly longer than that of

rsEGFP2 (Figure 1d, e) but much shorter than that of rsEGFP(N205S), which enables GMars-T a good RSFP for fast RESOLFT nanoscopy. Since the photobleaching of RSFPs from Anthozoan species under low and high switching light could adopt different pathways,[24] we then measured the photofatigue resistance of GMars-T in live cells over 3000 switching cycles at low intensity switching light (405nm, 25W/cm^2, 488nm, 50W/cm^2) and 2000 switching cycles at high intensity switching light (405nm, 0.1kW/cm^2, 488nm, 1kW/cm^2). The data showed that under low switching light (Figure 1f), GMars-T showed significantly higher photofatigue resistance than rsEGFP(N205S) while under high switching light (Figure S2), the photofatigue resistant of GMars-T is more similar as rsEGFP(N205S).[5,23]

Apart from the aforementioned properties, GMars-T was also monomeric (Figure S3). We then explored the applications of GMars-T in various subcellular structures and organelles using a parallelized RESOLFT microscope (Figure 2a-e). The effective spatial resolution was quantified by measuring intensity profiles of intracellular filamentous structures such as EB3-GMars-T labeled microtubules. The full width at half maximum (FWHM) indicates a resolution of ~80 nm under relative low turn-off laser power (~1kW/cm^2) (Figure. 2f-j, Figure S4).

Interestingly, GMars-T also demonstrated rapid and stochastic intensity fluctuations in live cells at single pixel level upon simultaneous illumination with 405nm (~10W/cm^2) and 488nm (~100W/cm^2) light, similar as previously reported blinking behavior of Dronpa.[13] Therefore, in addition to RESOLFT imaging, we also sought to evaluate GMars-T for pcSOFI imaging in live cells. After transfection of Lifeact-GMars-T, live HeLa cells displayed a bright fluorescence distribution characteristic of the actin cytoskeleton. We acquired 500 images over approximately 1 s using a high speed sCMOS camera and subjected these to a second-order cross-cumulant pcSOFI analysis. The resulting image displayed a 2-fold increase in spatial resolution (Figure 3a-e, Figure S5) and moreover, long-term live-cell super-resolution visualization of actin dynamics could also be reached at high temporal resolution (~1 s/frame) (Movie S1, Movie S2). These features make GMars-T a great fluorescent probe with multimodal super-resolution imaging

capability.

Apart from multimodal super-resolution structural imaging revealing fine subcellular structures demonstrated above, we wonder whether GMars-T could be used for functional imaging reporting PPIs in live cells based on its derived bimolecular fluorescence complementation biosensor.[25] To determine the optimal cleavage site for generating non-fluorescent fragments of GMars-T for BiFC imaging, we referred to mEos3.2 which was previously used in establishing BiFC assay[26] with a cleavage site between 164E and 165G, as the amino acids sequence of GMars-T shares 80% identity with that of mEos3.2 (Figure S6a). We then used β-Fos/β-Jun, a constitutive heterodimer interaction model[27] to test the reconstitution performance of split GMars-T between corresponding splitting site 173K and 174G. We fused the two fragments, GMars-T-N (residues 1-173aa) to the N-terminus of c-Jun residues 257-334aa (β-Jun) and GMars-T-C (residues 174-237aa) to the C-terminus of c-Fos residues 118-211aa (β-Fos), respectively (Figure S6b). β-Fos and β-Jun are known to form a heterodimer through leucine zipper interaction, which often serves as a model system to examine the fluorescence complementation of BiFC.[28] To test the specificity of GMars-T-based BiFC assay in detecting PPIs, we fused GMars-T-C (residues 174-237aa) to the C-terminus of β-Fos (Δ Zip), a β-Fos mutant with the interaction domain (residues 179-193aa) deleted. The flexible linker sequences were selected as 2×GGGGS between GMars-T-N and β-Jun and 4×GGGGS between β-Fos/β-Fos (Δ Zip) and GMars-T-C respectively. As shown in Figure 4, live HeLa cells coexpressing GMars-T-N-β-Jun and β-Fos-GMars-T-C showed bright reconstituted green fluorescence under 37 ℃ (Figure 4a), while HeLa cells cotransfected with GMars-T-N-β-Jun and β-Fos (ΔZip)-GMars-T-C showed extremely low spontaneously reconstituted green fluorescence signal that was not significantly different from the background fluorescence produced by non-transfected cells (Figure 4b), which indicated very high specific BiFC signal for detecting PPIs under physiological temperature in live mammalian cells using GMars-T-based BiFC system. Quantitatively measured by fluorescence spectrophotometer, ensemble fluorescence of live HeLa cells coexpressing GMars-T-N-β-Jun and β-Fos-GMars-T-C were over

25 times brighter than that of cells coexpressing GMars-T-N-β-Jun and β-Fos (ΔZip)-GMars-T-C under physiological conditions (Figure 4c,d), indicating that GMars-T-based BiFC assay has the largest imaging contrast than previously established classical BiFC reporters derived from GFP variants.[29] Additionally, most biochemical and photophysical characteristics of complemented GMars-T were also reserved (Figure S7). Moreover, the high specificity and sensitivity of GMars-T-based BiFC assay (Figure S8) were also confirmed by rapamycin-inducible FRB/FKBP interaction system.[30]

In order to test the performance of GMars-T-based BiFC assay in detection and visualization of various PPIs at physiological conditions in live mammalian cells, we used five previously well-characterized protein-protein interaction (PPI) pairs: β-Fos/β-Jun, β-Fos/Jun,[31] Bcl-X_L/Bak,[32] actin/cofilin[33] and homodimerization of Lifeact targeting to polymerized G-actin.[34] In all the tested PPI pairs, bright green fluorescence could be readily detected in Live HeLa cells under 37℃ physiological temperature after 24 hours of plasmids transfection. Without any protein aggregations or mislocalization, the specific cellular distributions of PPI pairs could be visualized which are also in accordance with previous reports (Figure 5a-e, Figure S9). Those results all indicate that GMars-T-based BiFC assay can be readily used to detect and visualize various PPIs at different subcellular compartments. Moreover, combining with RESOLFT nanoscopy, the specific mitochondria membrane localization of Bcl-X_L/Bak interaction pair could also be revealed with high spatial resolution (Figure 5f).

Although GMars-T-based BiFC assay has been developed in this work, it also should note that as most previously established FP-based BiFC assays,[31] this newly developed RSFP-based BiFC assay is also irreversible, it can't be used to analyze the dissociation of two molecules. More efforts are still awaited for further optimizing FP-based BiFC assays along this direction.[29]

The development and applications of genetically-encoded fluorescent proteins and fluorescent protein-based biosensors have greatly revolutionized cell biology research at both structural imaging and functional imaging levels. As a special kind of

"smart fluorophores", the development and applications of RSFPs or RSFP-based biosensors has gained great attentions during recent years mainly because such probes coupled with various kinds of nanoscopy approaches enable fluorescence imaging and biosensing beyond diffraction limit. However, various live cell nanoscopy approaches have different strengths and weaknesses.[35-37]

In recent years, although various super-resolution imaging approaches including stochastic optical reconstruction microscopy (STORM),[38] photoactivated localization microscopy (PALM),[39] structured illumination microscopy (SIM),[40] nonlinear SIM (NSIM),[41,42] stimulated emission depletion (STED)[43], reversible saturable optical fluorescence transitions (RESOLFT) microscopy[12] and stochastic optical fluctuation imaging (SOFI)[44] with different characteristics have already been established, no single approach can satisfy various kinds of biological research in all terms, especially to live-cell nanoscopy approaches, their performances are still under debate and also need further optimization.[45,46] Thus, it can never be too cautious especially to inexperienced microscope users who are lack of sufficient knowledge to judge and interpret the imaging results. Since compared with super-resolution imaging approaches such as PALM/STORM mostly conducted with fixed dead cells, the super-resolution imaging results from NSIM, RESOLFT or pcSOFI mostly conducted with live cells are prone to suffer from even more complicated artifacts such as cell physical and physiological changes under different light illumination power,[47] photophysics of probe itself [48,49] and reconstruction artifacts during image post-processing.[50] Thus, there is an urgent need for probes cable of multimodal live-cell super-resolution imaging under different experimental conditions which could enable data cross-validation, and further combined with parallelly conducted biological controls and growing raft of tools to avoid artifacts.[51] For example, although RESOLFT nanoscopy approach such as parallelized RESOLFT microscopy offers robust real-time live cell imaging with 3~4 folds resolution improvement in large fields of view (100μm × 100μm), the relatively high power density of switching light (~1-10 kW/cm^2) not only put stringent requirements for the limited number of available highly photofatigue resistant RSFPs with specific photoswitching characteristics,[4,5] but also

lead to higher phototoxicity and photodamage for long-term live cell imaging.[47,52] In contrast, although photochromic stochastic optical fluctuation imaging (pcSOFI) is more tolerant of the imaging conditions and simultaneously with 10~100 folds lower power density of switching light (~100W/cm^2) than RESOLFT, which enables more friendly and longer time-lapse live cell imaging, it offers comparably lower spatial resolution improvement with an extra step for post image processing and analysis. Although such different strengths and weaknesses often allow high degree of complementarity, the complementarity afforded by the different nanoscopy approaches remains highly constrained by the lack of labels with multimodal fluorescence properties.[9] Thus, fluorescent probe such as RSFPs with multimodal super-resolution imaging capabilities are highly valuable, because such probes not only can facilitate convenient choice and flexible combination of nanoscopy approaches with different pros and cons according to the specific questions to be addressed, but also enable multiple cross-validation of large experimental data sets recording under different imaging conditions with different nanoscopy approaches.

To address this need, in this work, we developed GMars-T, a single green RSFP probe with both multimodal super-resolution structural imaging and high specificity functional imaging capabilities. Except from large on-off contrast ratio in live cells as previously reported GMars-Q, GMars-T is an even brighter and highly efficient photoswitching RSFP cable of fast RESOLFT nanoscopy. As demonstrated in a commercial parallelized RESOLFT microscope, 3~4 folds improvement of spatial resolution down to ~80 nm could be readily achieved in live cells. Apart from the capability for RESOLFT nanoscopy, we also found GMars-T displays obvious stochastic photoswitching under wide-field illumination scheme at single pixel level. By taking advantage of such fluorescence property, [53,54] pcSOFI analysis could also be performed which enables long-term time-lapse live cell fluorescence imaging at super-resolution level. Besides multimodal super-resolution structural imaging which reveals fine subcellular structures beyond diffraction limit, we also developed GMars-T-based BiFC sensor reporting PPIs with high specificity in live cells. The high specificity and superb imaging contrast of GMars-T-based BiFC assay were also

confirmed by both previously well-established constitutive classic β-Fos/β-Jun heterodimer interaction model and rapamycin-inducible FRB/FKBP interaction system. Further experiments also indicated that GMars-T-based BiFC assay can be readily applied to detect and visualize various PPIs at different subcellular compartments with both high specificity and high spatiotemporal resolutions. Thus, all of the data suggested that GMars-T is an excellent RSFP probe cable of both multimodal and multilevel fluorescence imaging in live cells.

Besides fluorescence imaging discussed above, it is also interesting to note that GMars-T displays dramatically different biophysical and photophysical properties such as p*K*a, photoswitching kinetics, photofatigue resistance from GMars-Q[55] owing to only one amino acid substitution at the first amino acid of its chromophore tripeptide (GMars-T, TYG, GMars-Q, QYG). Thus, GMars-Q and GMars-T is also a great pair of research subjects for studying structure and photophysics of RSFPs. We expect further investigations including protein crystal structure determination and comparable analysis could uncover the structure-function relationship which in-turn laid the basis for further structure-guided RSFPs design and application with desired fluorescence properties.[16]

CONCLUSIONS

In this work, we have generated a green RSFP, GMars-T which exhibits advantageous properties for both RESOLFT and pcSOFI super-resolution imaging in live cells. Additionally, we also generated high specificity BiFC sensor based on GMars-T for detection and visualization PPIs with high spatiotemporal resolution. As previously developed pcDronpa2[9] with multimodal subdiffraction imaging capability, the development and application of GMars-T will further expand the extremely valuable but limited RSFP toolbox specifically with multimodal and multilevel imaging capabilities.

REFERENCES

(1) Rodriguez, E. A.; Campbell, R. E.; Lin, J. Y.; Lin, M. Z.; Miyawaki, A.; Palmer, A. E.; Shu, X.; Zhang, J.; Tsien, R. Y. *Trends Biochem Sci* **2017**, *42*, 111-129.

(2) Zhang, M.; Chang, H.; Zhang, Y.; Yu, J.; Wu, L.; Ji, W.; Chen, J.; Liu, B.; Lu, J.; Liu, Y.; Zhang, J.; Xu, P.; Xu, T. *Nat Methods* **2012**, *9*, 727-729.

(3) Wang, S.; Moffitt, J. R.; Dempsey, G. T.; Xie, X. S.; Zhuang, X. *Proc Natl Acad Sci U S A* **2014**, *111*, 8452-8457.

(4) Grotjohann, T.; Testa, I.; Reuss, M.; Brakemann, T.; Eggeling, C.; Hell, S. W.; Jakobs, S. *Elife* **2012**, *1*, e00248.

(5) Wang, S.; Chen, X.; Chang, L.; Xue, R.; Duan, H.; Sun, Y. *ACS Nano* **2016**, *10,* 9136–9144.

(6) Duwé, S.; De Zitter, E.; Gielen, V.; Moeyaert, B.; Vandenberg, W.; Grotjohann, T.; Clays, K.; Jakobs, S.; Van Meervelt, L.; Dedecker, P. *ACS Nano* **2015**, *9*, 9528-9541.

(7) Zhang, X.; Chen, X.; Zeng, Z.; Zhang, M.; Sun, Y.; Xi, P.; Peng, J.; Xu, P. *ACS Nano* **2015**, *9*, 2659-2667.

(8) Zhang, X.; Zhang, M.; Li, D.; He, W.; Peng, J.; Betzig, E.; Xu, P. *Proc Natl Acad Sci U S A* **2016**, *113*, 10364-10369.

(9) Moeyaert, B.; Nguyen Bich, N.; De Zitter, E.; Rocha, S.; Clays, K.; Mizuno, H.; van Meervelt, L.; Hofkens, J.; Dedecker, P. *ACS Nano* **2014**, *8*, 1664-1673.

(10) Grotjohann, T.; Testa, I.; Leutenegger, M.; Bock, H.; Urban, N. T.; Lavoie-Cardinal, F.; Willig, K. I.; Eggeling, C.; Jakobs, S.; Hell, S. W. *Nature* **2011**, *478*, 204-208.

(11) Brakemann, T.; Stiel, A. C.; Weber, G.; Andresen, M.; Testa, I.; Grotjohann, T.; Leutenegger, M.; Plessmann, U.; Urlaub, H.; Eggeling, C.; Wahl, M. C.; Hell, S. W.; Jakobs, S. *Nat Biotechnol* **2011**, *29*, 942-947.

(12) Hofmann, M.; Eggeling, C.; Jakobs, S.; Hell, S. W. *Proc Natl Acad Sci U S A* **2005**, *102*, 17565-17569.

(13) Dedecker, P.; Mo, G. C.; Dertinger, T.; Zhang, J. *Proc Natl Acad Sci U S A* **2012**, *109*, 10909-10914.

(14) Hell, S. W.; Dyba, M.; Jakobs, S. *Curr Opin Neurobiol* **2004**, *14*, 599-609.

(15) Geissbuehler, S.; Dellagiacoma, C.; Lasser, T. *Biomed Opt Express* **2011**, *2*, 408-420.

(16) Adam, V.; Moeyaert, B.; David, C. C.; Mizuno, H.; Lelimousin, M.; Dedecker, P.; Ando, R.; Miyawaki, A.; Michiels, J.; Engelborghs, Y.; Hofkens, J. *Chem Biol* **2011**, *18*, 1241-1251.

(17) Adam, V.; Lelimousin, M.; Boehme, S.; Desfonds, G.; Nienhaus, K.; Field, M. J.; Wiedenmann, J.; McSweeney, S.; Nienhaus, G. U.; Bourgeois, D. *Proc Natl Acad Sci U S A* **2008**, *105*, 18343-18348.

(18) Chang, H.; Zhang, M.; Ji, W.; Chen, J.; Zhang, Y.; Liu, B.; Lu, J.; Zhang, J.; Xu, P.; Xu, T. *Proc Natl Acad Sci U S A* **2012**, *109*, 4455-4460.

(19) Chudakov, D. M.; Verkhusha, V. V.; Staroverov, D. B.; Souslova, E. A.; Lukyanov, S.; Lukyanov, K. A. *Nat Biotechnol* **2004**, *22*, 1435-1439.

(20) Lavoie-Cardinal, F.; Jensen, N. A.; Westphal, V.; Stiel, A. C.; Chmyrov, A.; Bierwagen, J.; Testa, I.; Jakobs, S.; Hell, S. W. *Chemphyschem* **2014**, *15*, 655-663.

(21) Guizar-Sicairos, M.; Thurman, S. T.; Fienup, J. R. *Opt Lett* **2008**, *33*, 156-158.

(22) Dedecker, P.; Duwé, S.; Neely, R. K.; Zhang, J. *J Biomed Opt* **2012**, *17*, 126008.

(23) Chmyrov, A.; Keller, J.; Grotjohann, T.; Ratz, M.; d'Este, E.; Jakobs, S.; Eggeling, C.; Hell, S. W. *Nat Methods* **2013**, *10*, 737-740.

(24) Duan, C.; Adam, V.; Byrdin, M.; Ridard, J.; Kieffer-Jaquinod, S.; Morlot, C.; Arcizet, D.; Demachy, I.; Bourgeois, D. *J Am Chem Soc* **2013**, *135*, 15841-15850.

(25) Wang, S.; Ding, M.; Chen, X.; Chang, L.; Sun, Y. *Biomed Opt Express* **2017**, *8*, 3119-3131.

(26) Liu, Z.; Xing, D.; Su, Q. P.; Zhu, Y.; Zhang, J.; Kong, X.; Xue, B.; Wang, S.; Sun, H.; Tao, Y.; Sun, Y. *Nat Commun* **2014**, *5*, 4443.

(27) Hu, C. D.; Chinenov, Y.; Kerppola, T. K. *Mol Cell* **2002**, *9*, 789-798.

(28) Shyu, Y. J.; Liu, H.; Deng, X.; Hu, C. D. *Biotechniques* **2006**, *40*, 61-66.

(29) Kodama, Y.; Hu, C. D. *Biotechniques* **2012**, *53*, 285-298.

(30) Banaszynski, L. A.; Liu, C. W.; Wandless, T. J. *J Am Chem Soc* **2005**, *127*, 4715-4721.

(31) Hu, C. D.; Kerppola, T. K. *Nat Biotechnol* **2003**, *21*, 539-545.

(32) Sattler, M.; Liang, H.; Nettesheim, D.; Meadows, R. P.; Harlan, J. E.; Eberstadt, M.; Yoon, H. S.; Shuker, S. B.; Chang, B. S.; Minn, A. J.; Thompson, C. B.; Fesik, S. W. *Science* **1997**, *275*, 983-986.

(33) Ohashi, K.; Kiuchi, T.; Shoji, K.; Sampei, K.; Mizuno, K. *Biotechniques* **2012**, *52*, 45-50.

(34) Riedl, J.; Crevenna, A. H.; Kessenbrock, K.; Yu, J. H.; Neukirchen, D.; Bista, M.; Bradke, F.; Jenne, D.; Holak, T. A.; Werb, Z.; Sixt, M.; Wedlich-Soldner, R. *Nat Methods* **2008**, *5*, 605-607.

(35) Nienhaus, K.; Nienhaus, G. U. *J Mol Biol* **2016**, *428*, 308-322.

(36) Cox, S. *Dev Biol* **2015**, *401*, 175-181.

(37) Schermelleh, L.; Heintzmann, R.; Leonhardt, H. *J Cell Biol* **2010**, *190*, 165-175.

(38) Rust, M. J.; Bates, M.; Zhuang, X. *Nat Methods* **2006**, *3*, 793-795.

(39) Betzig, E.; Patterson, G. H.; Sougrat, R.; Lindwasser, O. W.; Olenych, S.; Bonifacino, J. S.; Davidson, M. W.; Lippincott-Schwartz, J.; Hess, H. F. *Science* **2006**, *313*, 1642-1645.

(40) Gustafsson, M. G. *J Microsc* **2000**, *198*, 82-87.

(41) Gustafsson, M. G. *Proc Natl Acad Sci U S A* **2005**, *102*, 13081-13086.

(42) Li, D.; Shao, L.; Chen, B. C.; Zhang, X.; Zhang, M.; Moses, B.; Milkie, D. E.; Beach, J. R.; Hammer, J. A., 3rd; Pasham, M.; Kirchhausen, T.; Baird, M. A.; Davidson, M. W.; Xu, P.; Betzig, E. *Science* **2015**, *349*, aab3500.

(43) Klar, T. A.; Jakobs, S.; Dyba, M.; Egner, A.; Hell, S. W. *Proc Natl Acad Sci U S A* **2000**, *97*, 8206-8210.

(44) Dertinger, T.; Colyer, R.; Iyer, G.; Weiss, S.; Enderlein, J. *Proc Natl Acad Sci U S A* **2009**, *106*, 22287-22292.

(45) Sahl, S. J.; Balzarotti, F.; Keller-Findeisen, J.; Leutenegger, M.; Westphal, V.; Egner, A.; Lavoie-Cardinal, F.; Chmyrov, A.; Grotjohann, T.; Jakobs, S. *Science* **2016**, *352*, 527.

(46) Li, D.; Betzig, E. *Science* **2016**, *352*, 527.

(47) Waldchen, S.; Lehmann, J.; Klein, T.; van de Linde, S.; Sauer, M. *Sci Rep* **2015**,

5, 15348.

(48) Peeters, Y.; Vandenberg, W.; Duwé, S.; Bouwens, A.; Lukes, T.; Ruckebusch, C.; Lasser, T.; Dedecker, P. *Sci Rep* **2017**, *7*, 10470.

(49) Vandenberg, W.; Dedecker, P. *Sci Rep* **2017**, *7*, 44665.

(50) Heintzmann, R.; Huser, T. *Chem Rev* **2017**, *117*, 13890-13908.

(51) Culley, S.; Albrecht, D.; Jacobs, C.; Pereira, P. M.; Leterrier, C.; Mercer, J.; Henriques, R. *Nat Methods* **2018**.

(52) Strack, R. *Nat Methods* **2015**, *12*, 1111.

(53) Duwé, S.; Moeyaert, B.; Dedecker, P. *Curr Protoc Chem Biol* **2015**, *7*, 27-41.

(54) Moeyaert, B.; Dedecker, P. *Methods Mol Biol* **2014**, *1148*, 261-276.

(55) Nienhaus, K.; Nienhaus, G. U. *ACS Nano* **2016**, *10,* 9104–9108.

ASSOCIATED CONTENT

Supporting Information

The Supporting Information is available free of charge on the ACS Publications website http://pubs.acs.org.

Experimental details and data (PDF)

Time-lapse wide-field imaging of a living HeLa cell expressing Lifeact-GMars-T (AVI)

Time-lapse pcSOFI imaging of a living HeLa cell expressing Lifeact-GMars-T (AVI)

Author Contributions

S.W. and Y.S. designed the project. S.W. performed protein mutation and applications. S.W., X.C., L.C., M.D., R.X. and H.D. performed protein characterization. S.W. and Y.S. wrote the manuscript.

Notes

The authors declare no competing financial interest.

ACKNOWLEDGMENTS

We are grateful to Professor X.W. Zhuang (Department of Chemistry and Chemical Biology, Harvard University) for providing mMaple3 plasmid; Professor N. Yan, X.J. Pan, and W.Y. Huang (School of Life Sciences and School of Medicine, Tsinghua University) for their support in protein purification and dimerization tendency assay; Professor Q.H. He (Peking University Health Science Center) for aid in operating the Leica microscope; Professor W.S. Wei (School of Life Sciences, Peking University) for providing microplate reader (Infinite 200, Tecan); and S. Qiao (School of Life Sciences, Peking University) for technical support of fluorescence measurements. This work is supported by grants from the National Key R&D Program of China, No. 2017YFA0505300, and the National Science Foundation of China 21390412, , and 31327901 for Y.S.

Figures and legends

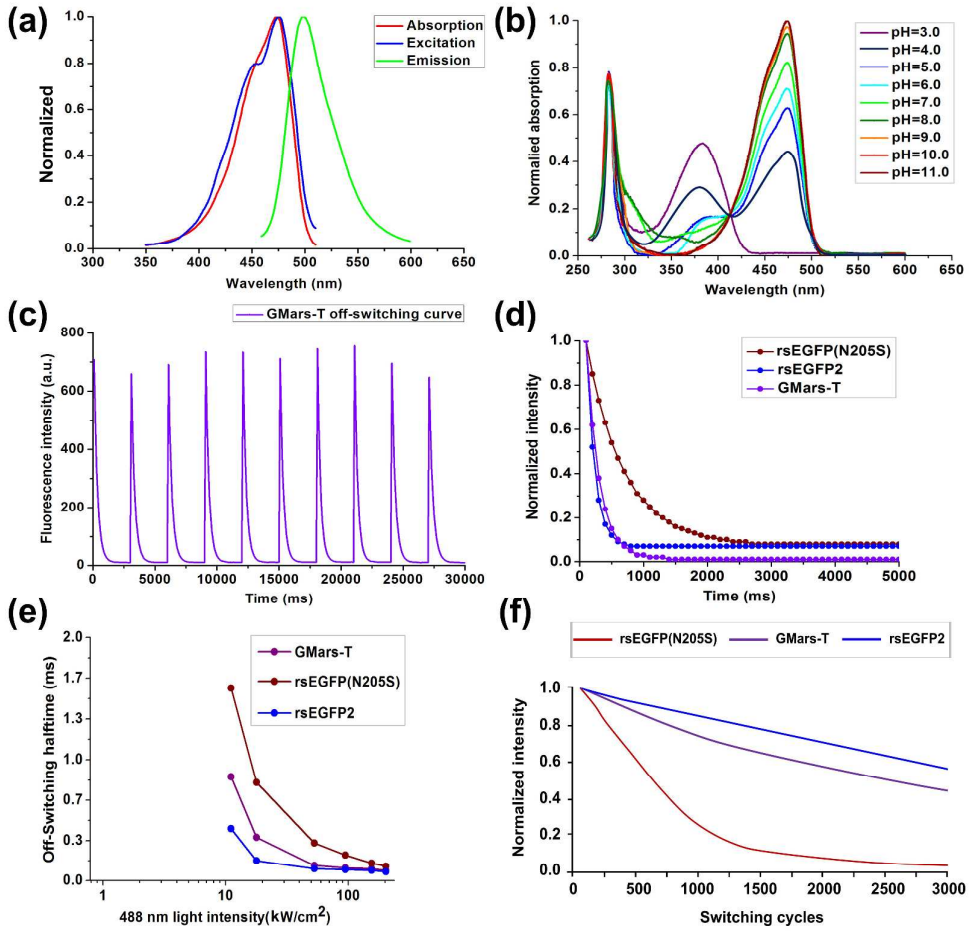

Figure 1 Characterization of GMars-T.

(a) Absorption (red), excitation (blue, maximum 476 nm), and emission (green, maximum 498 nm) spectra of GMars-T in its equilibrium state at pH7.5. (b) Absorption spectra of GMars-T at different pH values. (c) 10 consecutive off-switching curves of GMars-T in live cells by alternating irradiation with 405 nm light (25 W/cm^2, 100 ms) and 488 nm (50 W/cm^2, 3000 ms). The off-switching time constant (τ) was determined about 400 ms by fitting the curves. (d) Ensemble off-switching curves of GMars-T, rsEGFP2 and rsEGFP(N205S) in live cells by alternating irradiation with 488 nm (50 W/cm^2, 5000 ms) and 405 nm light (25 W/cm^2, 100 ms). (e) Comparison of the ensemble off-switching halftimes of GMars-T, rsEGFP2 and rsEGFP(N205S) at different high 488 nm light intensities. On-switching 405 nm light was kept constant (2 kW/cm^2). (f) Switching fatigue of GMars-T, rsEGFP2 and rsEGFP(N205S) in live cells by alternating irradiation with 488 nm (50 W/cm^2, 3000 ms) and 405 nm light (25 W/cm^2, 100 ms). Illumination times were chosen so that the fluorescence was fully switched to the minimum or maximum respectively in each cycle. Data were presented as averaged data from three independent experiments.

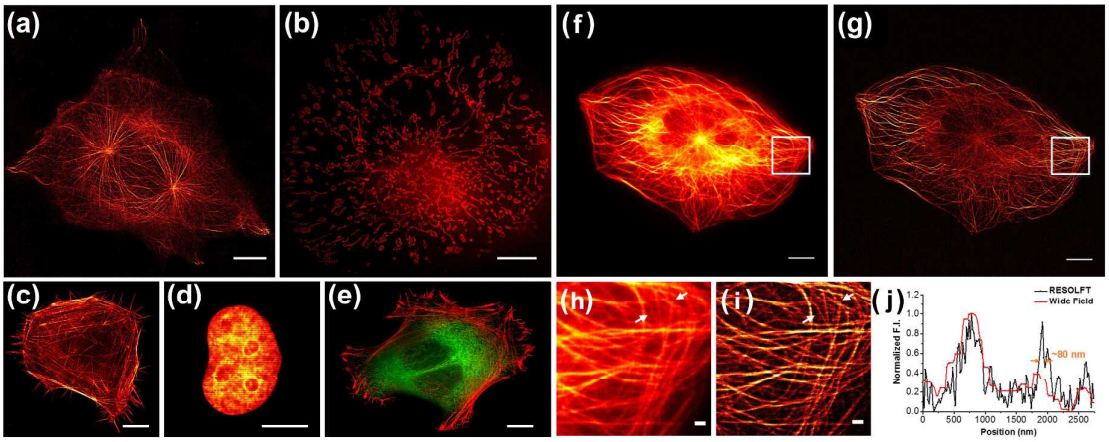

Figure 2 Expression and characterization of various functional GMars-T fusion proteins in live mammalian cells by a parallelized RESOLFT microscope.

(a-e) expression of various GMars-T fusion proteins in live mammalian cells; (a) EB3-GMars-T (targeting to microtubules) in U2OS cell; (b) Mito-GMars-T (targeting to mitochondria) in HeLa cell; (c) Lifeact-GMars-T (targeting to actin filaments) in HeLa cell; (d) H2B-GMars-T in HeLa cell; (e) Lifeact-rsCherryRev1.4 (red) and GMars-T-KDEL (green, targeting to ER) in HeLa cell. (f-j) characterization of the spatial resolution of GMars-T by a cellular filamentous structure; (f) conventional wide-field image of U2OS cell expressing EB3-GMars-T (targeting to microtubule filaments), (g) RESOLFT image of (f), (h) magnified image of the boxed area of (f), (i) magnified image of the box area of (g), (j) intensity profiles measured of arrowed regions in (h) and (i); Scale bar: 5 μm in (a-e); 10 μm in (f, g); 1 μm in (h, i). In Figure 2a-e, 36 nm scanning step (pixel) size was used for RESOLFT image reconstruction. In Figure 2g, 20nm scanning step (pixel) size was used for RESOFLT image reconstruction and resolution quantification. A 405 nm continuous wave diode laser was used for on-switching (2 ms; 12 mW measured at the back focal plane of the objective); a 488 nm continuous wave laser was used for off-switching (15 ms; 50 mW measured at the back focal plane of the objective) and fluorescence readout (4 ms; 50 mW measured at the back focal plane of the objective).

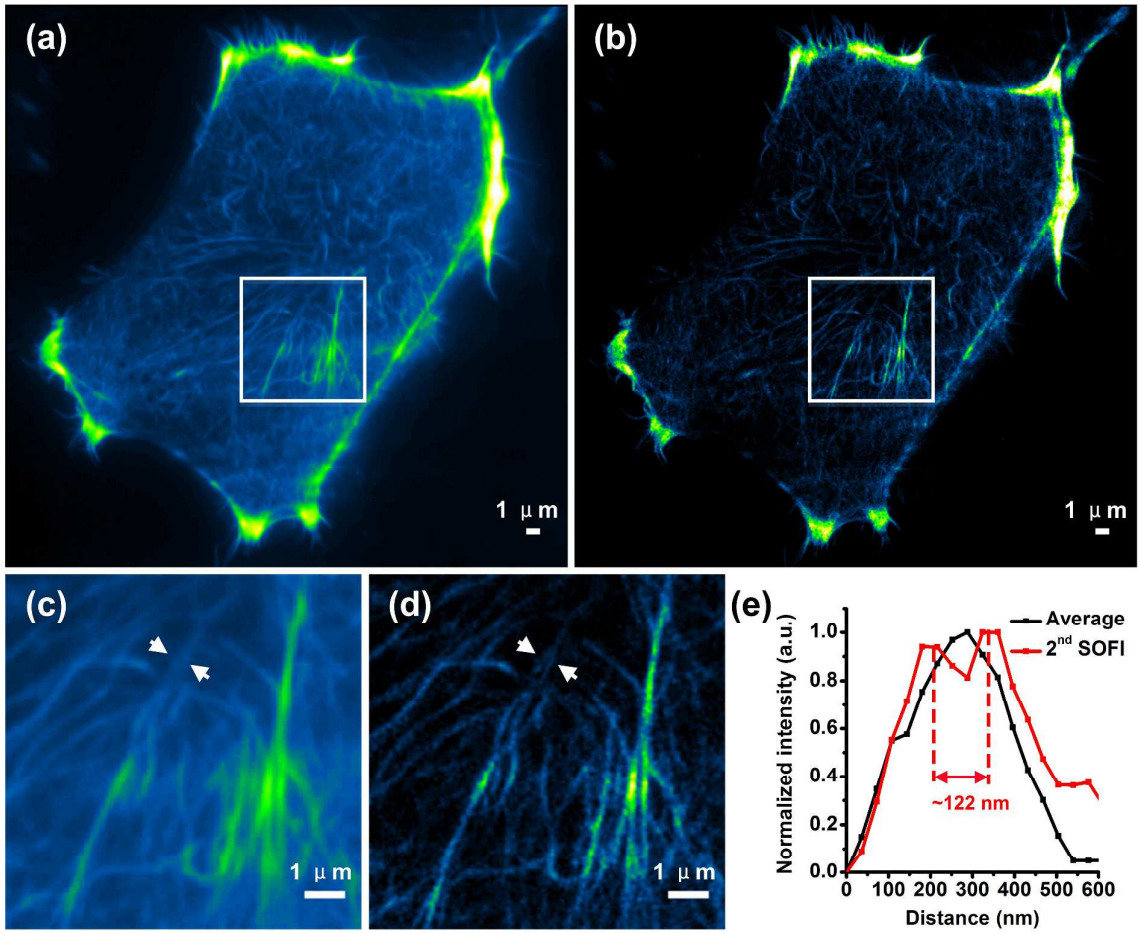

Figure 3 Fluorescence and corresponding SOFI images of a living HeLa cell expressing GMars-T fused with Lifeact.

(a) Average of original 500 fluorescence frames, and the exposure time was 2 ms per frame. (b) Second-order SOFI image obtained through the analysis of the same 500 frames. (c, d) Zoomed-in views of the boxed regions in (a) and (b), respectively; (e) Intensity profiles of cross sections taken along the two white arrowheads indicated in (c) and (d).Scale bar: 1μm.

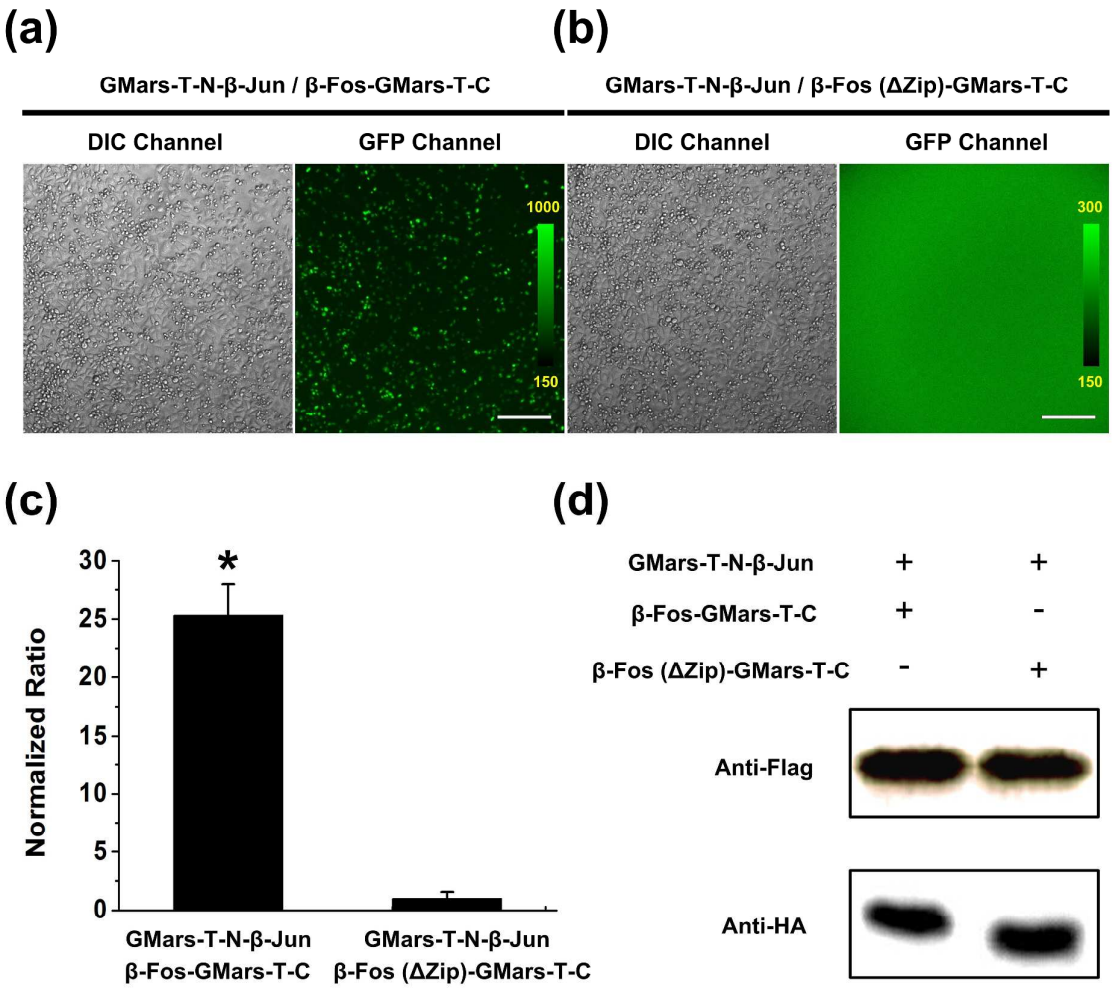

Figure 4 Split GMars-T for BiFC analysis in live HeLa cells.

HeLa cells individually coexpressing (a) GMars-T-N- β-Jun, β-Fos-GMars-T-C and mCherry (internal control to normalize expression levels) or (b) coexpressing GMars-T-N-β-Jun, β-Fos(ΔZip)-GMars-T-C and mCherry were imaged under a fluorescence microscope equipped with a 10 × objective lens in both DIC channel and GFP channel. Scale bar: 200μm. The intensity scale of GFP channel was displayed from 150 to 1000 for (a) or 150 to 300 for (b) respectively. The relative ensemble brightness (ratio) of cells expressing indicated plasmids were measured with fluorescence spectrophotometer in (c), *$p<0.01$ compared with cells coexpressing GMars-T-N-β-Jun, β-Fos(ΔZip)-GMars-T-C and the data were from three independent measurements and expressed as means±SD values. (d) Comparable expression level of the fusion proteins in (a) and (b) determined by western blotting with anti-Flag and anti-HA antibodies.

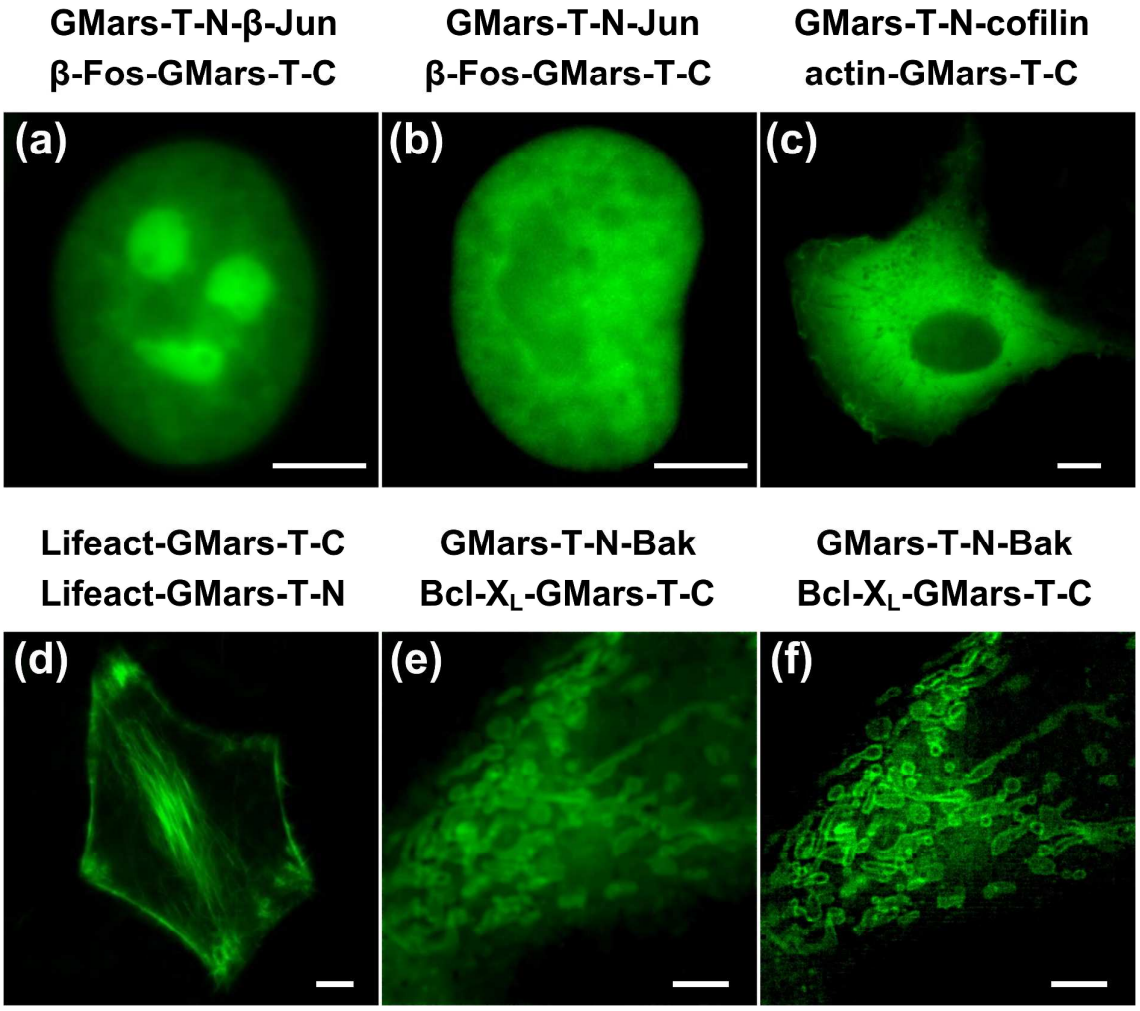

Figure 5 Detecting and visualizing various protein-protein interactions at different subcellular compartments with GMars-T-based BiFC.

Conventional wide-field fluorescence images of HeLa cells detecting and visualizing (a) β-Jun/β-Fos, (b) β-Fos/Jun, (c) actin/cofilin, (d) Lifeact/Lifeact targeting to polymerized G-actin and (e) Bak/Bcl-X_L interactions by GMars-T-based BiFC assay. (f) Parallelized RESOLFT image of (e).Scale bar: 5μm.

For Toc graph only: